Attahadi Medical Journal
2026;3(3):471-487
https://doi.org/10.69667/amj.26330

OPEN ACCESS

Original article

Mathematical Modeling, Bio-Dynamic Analysis, and Optimal Control of Periodontal Disease Progression Incorporating Time Delays, Host-Modulation Therapy, and Realistic Clinical Scenarios

Emad Awadh[1], Ayoub Akgam[2]

[1] Department of Mathematics, Faculty of Science, Tobruk University, Tobruk, Libya
[2] Faculty of Oral and Dental Medicine, University of Benghazi, Benghazi, Libya
Email: emad.awadh@tu.edu.ly

Keywords.
Periodontitis; Delay Differential Equations; Host-Modulation Therapy; Hopf Bifurcation; Basic Reproduction Number.

A B S T R A C T

Periodontitis is a chronic multi-factorial inflammatory condition characterized by subgingival dysbiosis and immunopathological tissue breakdown, ultimately leading to connective-tissue attachment loss and alveolar bone resorption. This paper extends a previously formulated four-dimensional ordinary differential equation (ODE) model of subgingival bacterial biofilm, neutrophil/cytokine dynamics, tissue damage, and local antimicrobial pharmacokinetics into a five-dimensional delay-differential-equation (DDE) framework that (i) incorporates a physiologically realistic lag τ1 in immune-cell activation and a lag τ2 in the onset of tissue-repair signalling, and (ii) introduces an explicit host-modulation therapy (HMT) compartment ν(t) — representing, e.g., a sub-antimicrobial-dose MMP-inhibitor — that suppresses the bystander immunopathological damage coefficient β2 through a saturating inhibition law. Beyond the original stability theory (disease-free/endemic equilibria, Lyapunov/LaSalle global stability, R0 via the Next-Generation-Matrix method), we perform an equilibrium-continuation bifurcation analysis of the (B, I) subsystem across the R0 = 1 threshold and a closed-form delay-induced Hopf bifurcation analysis of the immune-activation lag τ1, identifying the critical delay τ1* beyond which sustained inflammatory oscillations emerge — a candidate mechanistic explanation for cyclical, flare-and-remission patterns observed clinically in chronic periodontitis. A dual optimal-control problem (local antimicrobial S1(t) and host-modulation S2(t)) is solved via Pontryagin's Minimum Principle and a Forward-Backward Sweep numerical scheme. Two new clinically motivated scenarios — a smoker phenotype with delayed immune kinetics, and a diabetic host under optimal dual therapy — are added to the original three scenarios. An extended Latin-Hypercube/PRCC sensitivity analysis (now spanning nine parameters, including τ1, τ2 and the HMT potency κ) confirms host susceptibility (σ) and bystander immune damage (β2) as dominant drivers of bone loss, while showing that HMT potency (κ) is itself a strong protective factor (PRCC ≈ −0.74). Numerical results show that combining antimicrobial and host-modulation control lowers day-60 cumulative tissue damage from D(60) ≈ 0.96 (antimicrobial alone) to D(60) ≈ 0.66 in a poorly controlled diabetic host — a clinically meaningful improvement that is preserved once realistic immune/repair delays are reintroduced.

Introduction

Periodontal disease affects up to half of the global adult population and is one of the leading causes of tooth loss worldwide [1, 2]. The condition is initiated by a shift from a symbiotic oral microbiome to a dysbiotic, pathogenic biofilm dominated by red-complex bacteria such as Porphyromonas gingivalis, Tannerella forsythia, and Treponema denticola [3, 4]. Rather than direct bacterial cytotoxicity alone, contemporary models of periodontal pathogenesis emphasize that the majority of irreversible matrix breakdown and alveolar bone loss stems from an over-activated, dysregulated host immune response — bystander tissue destruction driven by IL-1β, TNF-α, IL-6, and matrix metalloproteinases (MMPs) [5, 6].

Systemic co-factors, such as uncontrolled Type 2 diabetes mellitus, chronic psychological stress, and heavy smoking, significantly amplify host inflammatory susceptibility, accelerating disease progression [7, 8, 9]. Two additional biological features motivate the extension developed in this paper. First, neutrophil recruitment and activation is not instantaneous: chemotactic signalling, transendothelial migration, and clonal mobilization of immune effectors introduce a lag on the order of one to several days between a bacterial challenge and the peak host response [10, 11]. Second, host-modulation therapy — sub-antimicrobial-dose doxycycline and other MMP-inhibiting or cytokine-targeting adjuncts — is now an established adjunct to mechanical debridement in clinical periodontology, acting directly on the bystander-damage pathway rather than on the bacteria themselves [12, 13, 14]. Neither delayed immune kinetics nor host-modulation therapy were represented in the original four-compartment ODE model.

Received*: 26-06-2026 -* ***Accepted****: 25-08-2026 -* ***Published****: 02-09-2026*

Attahadi Medical Journal
2026;3(3):471-487
https://doi.org/10.69667/amj.26330

The primary contributions of this extended paper are:

- Reformulating the immune-activation and tissue-repair equations as delay differential equations (DDEs) with lags τ1 and τ2, integrated via a method-of-steps Runge–Kutta scheme;
- Introducing a fifth state variable v(t) representing host-modulation therapy concentration, which suppresses the bystander damage coefficient β2 through a saturating Hill-type inhibition;
- Performing an equilibrium-continuation bifurcation study of the (B, I) subsystem to test for backward-bifurcation-type bistability across R0 = 1, and a closed-form Hopf-bifurcation analysis identifying the critical immune-activation delay τ1* at which sustained inflammatory oscillations emerge;
- Formulating and numerically solving a dual optimal-control problem (Pontryagin's Minimum Principle, Forward-Backward Sweep Method) that jointly optimizes local antimicrobial delivery S1(t) and host-modulation dosing S2(t);
- Adding two clinically motivated scenarios — a smoker phenotype with delayed immune kinetics, and a diabetic host under optimal dual therapy — and extending the PRCC global sensitivity analysis to the three new parameters (τ1, τ2, κ).

Mathematical Model Formulation

Let the temporal evolution of periodontal infection at time t (days) be governed by four continuous state variables:

- B(t) — pathogenic bacterial density in the subgingival pocket (cells/mL);
- I(t) — active host immune-cell (neutrophil) and cytokine density (cells/mL);
- D(t) — normalized cumulative periodontal tissue and alveolar bone damage, D(t) ∈ [0, 1];
- u(t) — concentration of active antimicrobial drug in the sulcular fluid (mg/L).

The coupled non-linear baseline system of differential equations is

$$\frac{dB}{dt} = rB\left(1 - \frac{B}{K}\right) - \gamma BI - \eta Bu(t) \qquad (1)$$

$$\frac{dI}{dt} = \alpha B\left(1 - \frac{I}{I_{\max}}\right) - \mu_i I \qquad (2)$$

$$\frac{dD}{dt} = \sigma\left(\beta_1 B + \beta_2 I\right)\left(1 - D\right) - \delta D \qquad (3)$$

$$\frac{du}{dt} = S(t) - \theta\, u(t) \qquad (4)$$

Equation (3) extends the originally proposed linear damage law

$$\dot{D} = \sigma\left(\beta_1 B + \beta_2 I\right) - \delta D$$

with a logistic saturation factor (1 − D). This enforces the biologically required bound D(t) ∈ [0, 1] for all admissible initial conditions and parameter values (a bounded "fraction of bone destroyed" cannot itself become unbounded), while leaving the qualitative interpretation of every term unchanged: direct enzymatic/toxin-mediated damage (σβ1B), bystander immunopathological damage (σβ2I), and first-order tissue repair (−δD).

Biological Interpretation of Parameters

Table 1 summarizes the biological meaning, units, and baseline values used throughout the paper (extended relative to the original model with the three new delay/therapy parameters τ1, τ2, κ, and the HMT washout rate θv). Figure 1 shows the updated mechanistic compartmental diagram, including the new v(t) compartment and both delay loops.

Table 1. Biological definition of model parameters and baseline values (new parameters marked NEW).

Description	Symbol	Baseline	Units	Biological meaning
Bacterial growth rate	r	0.75	day^{-1}	Intrinsic proliferation rate of pathogenic biofilm
Carrying capacity	K	10^7	cells/mL	Maximum bacterial load supported by the sulcular pocket
Immune clearance	γ	1.2×10^{-6}	$mL\cdot cell^{-1}\cdot day^{-1}$	Bacterial killing rate by host phagocytes
Drug efficacy	η	0.05	$L\cdot mg^{-1}\cdot day^{-1}$	Bacterial kill rate per unit antimicrobial concentration
Immune recruitment	α	0.08	day^{-1}	Rate of immune-cell activation per bacterial pathogen

Received: 26-06-2026 - **Accepted**: 25-08-2026 - **Published**: 02-09-2026

Attahadi Medical Journal
2026;3(3):471-487
https://doi.org/10.69667/amj.26330

Max. immune limit	I_max	10^6	cells/mL	Physiological saturation capacity of the immune response
Immune decay rate	μ_i	0.15	day^{-1}	Apoptosis/clearance rate of immune effectors
Direct damage rate	β1	1.0×10^{-8}	day^{-1}	Tissue degradation rate by bacterial toxins/enzymes
Indirect damage rate	β2	2.0×10^{-7}	day^{-1}	Bystander tissue breakdown by hyperactive immunity
Repair rate	δ	0.03	day^{-1}	Natural connective-tissue remodeling and repair rate
Host susceptibility	σ	1.0	dimensionless	Inflammatory hyper-reactivity factor (e.g., diabetes, smoking)
Drug washout rate	θu	0.40	day^{-1}	Clearance rate of antimicrobial via crevicular fluid flow
Immune-activation delay (NEW)	τ1	0 – 6	days	Lag between bacterial challenge and neutrophil/cytokine activation
Repair-onset delay (NEW)	τ2	0 – 8	days	Lag between damage signalling and remodeling/repair response
HMT potency (NEW)	κ	0 – 10	$L\cdot mg^{-1}$ (eff.)	Saturating suppression of β2 by host-modulation therapy v(t)
HMT washout rate (NEW)	θv	0.30	day^{-1}	Clearance rate of host-modulation agent

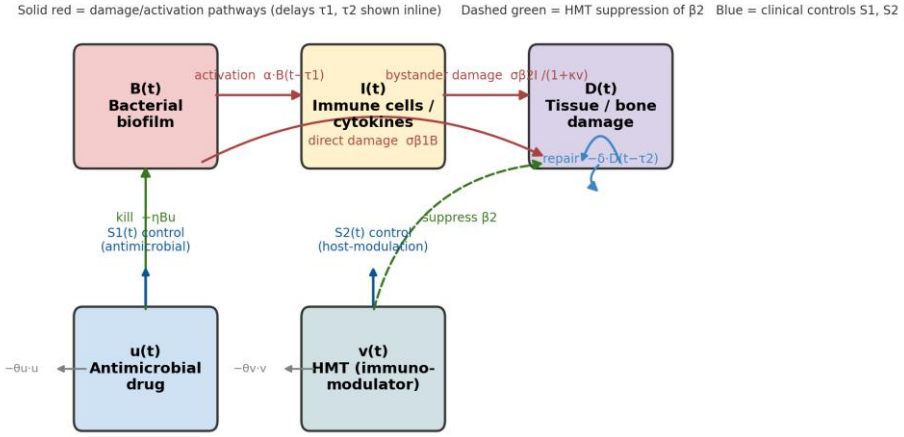

Figure 1. Updated mechanistic compartmental structure of the five-dimensional periodontal model. Red arrows show the (possibly delayed) activation and damage pathways; the dashed green arrow shows suppression of β2 by host-modulation therapy v(t); blue arrows show the two clinical controls S1(t) and S2(t).

Extended Model: Time-Delayed Immune/Repair Dynamics and Host-Modulation Therapy

Two biological refinements are introduced. First, the recruitment and activation of neutrophils and pro-inflammatory cytokines is not instantaneous: we replace the instantaneous bacterial signal αB(t) in Eq. (2) with the delayed signal αB(t − τ1), where τ1 (days) represents the time required for chemotactic signalling and clonal immune-cell mobilization. Second, the onset of tissue-repair/remodeling in response to a given damage state is itself delayed by τ2 (days), reflecting the time required to initiate osteoblastic/fibroblastic remodeling once a damage signal has been sustained; we implement this by delaying the repair term to −δD(t − τ2).

Third, we introduce a host-modulation therapy (HMT) compartment v(t) — representing, for example, a sub-antimicrobial-dose MMP-inhibitor such as SDD (sub-antimicrobial-dose doxycycline) [12, 13, 14] — governed by its own pharmacokinetic input/washout balance, dv/dt = S2(t) − θv v, where S2(t) is the clinician-controlled HMT dosing rate. Rather than acting on the bacteria, v(t) suppresses the bystander immunopathological damage coefficient β2 through a saturating (Hill-type) inhibition, β2/(1 + κv), where κ ≥ 0 is the HMT potency. This functional form guarantees β2,eff → 0 as v → ∞ while reducing exactly to the original model when v ≡ 0 (κ arbitrary) or κ = 0 (HMT ineffective).

The resulting five-dimensional delay-differential-equation (DDE) system, with state y = (B, I, D, u, v), is:

Received*: 26-06-2026 -* ***Accepted****: 25-08-2026 -* ***Published****: 02-09-2026*

Attahadi Medical Journal
2026;3(3):471-487
https://doi.org/10.69667/amj.26330

$$\dot{B} = r(t)\,B\left(1-\tfrac{B}{K}\right) - \gamma BI - \eta Bu$$
$$\dot{I} = \alpha\,B(t-\tau_1)\left(1-\tfrac{I}{I_{max}}\right) - \mu_i I$$
$$\dot{D} = \sigma\left(\beta_1 B + \tfrac{\beta_2 I}{1+\kappa V}\right)(1-D) - \delta\,D(t-\tau_2)$$
$$\dot{u} = S_1(t) - \theta_u u$$
$$\dot{v} = S_2(t) - \theta_v v$$

(Eq. 13)

Because no closed-form solution exists for non-linear DDE systems, Eq. (13) is integrated numerically using the method-of-steps: the delayed states B(t − τ1) and D(t − τ2) are obtained from a continuously updated, piecewise-linearly-interpolated solution history, and a classical fourth-order Runge–Kutta step is applied at each mesh point (Section 6). This scheme reduces exactly to the original non-delayed ODE integrator when τ1 = τ2 = 0, and to the original four-state system when additionally κ = 0 and v(0) = 0 (so that v(t) ≡ 0 for all t).

Rigorous Mathematical Analysis

Positivity and Invariance Region

Theorem 1 (Positivity and boundedness). *All trajectories originating in the non-negative hyper-octant $\mathbb{R}_{4+} = \{(B, I, D, u) \in \mathbb{R}^4 : B \geq 0, I \geq 0, D \geq 0, u \geq 0\}$ remain non-negative and bounded for all $t \geq 0$.*

Proof. Evaluating the vector field on each coordinate hyperplane gives

$$\left.\frac{dB}{dt}\right|_{B=0} = 0, \qquad \left.\frac{dI}{dt}\right|_{I=0} = \alpha B \geq 0 \quad \forall B \geq 0,$$

$$\left.\frac{dD}{dt}\right|_{D=0} = \sigma(\beta_1 B + \beta_2 I) \geq 0 \quad \forall B, I \geq 0, \qquad \left.\frac{du}{dt}\right|_{u=0} = S(t) \geq 0.$$

Since none of the vector-field components point outward across the boundary of $\mathbb{R}_{4+}$, the region is positively invariant. Standard comparison arguments applied to Eqs. (1) and (2) further give B(t) ≤ max{B(0), K} and I(t) ≤ max{I(0), I_max} for all t ≥ 0; since D(t) ∈ [0, 1] by construction of Eq. (3) and u(t) is driven by a bounded input S(t) with linear decay, all four state variables remain bounded. ■ The same argument extends directly to the delayed system (13): the delayed arguments B(t−τ1), D(t−τ2) inherit the same a priori bounds from the (non-delayed) history on [−max(τ1,τ2), 0], and v(t) is bounded by max{v(0), S2,max/θv} by the same comparison principle applied to du/dt.

Derivation of the Basic Reproduction Number R0

The disease-free equilibrium (DFE), obtained in the absence of any pre-existing infection and treatment (S(t) = 0), is E0 = (0, 0, 0, 0). Following the Next-Generation Matrix approach of van den Driessche and Watmough [15], we linearize the "new infection" component (rB, from the logistic growth term evaluated near B = 0) and the "transfer" component of the infected compartment I around E0. Since bacterial recruitment into the system is governed solely by the linear growth term rB and immune effectors decay at rate μ_i, the corresponding scalar next-generation matrices are

$$\mathcal{F} = [\,r\,], \qquad \mathcal{V} = [\,\mu_i\,]$$

$$R_0 = \frac{r}{\mu_i} \qquad (5)$$

Biological meaning. R0 represents the capacity of the pathogenic bacterial population to expand relative to the baseline rate at which host immune effectors are lost. R0 < 1 indicates that any small bacterial challenge is cleared faster than it can amplify the immune response; R0 > 1 indicates a self-sustaining infection capable of driving the system toward an endemic (chronic-disease) state.

Stability Analysis

Theorem 2 (Local stability). *If R0 < 1, the disease-free equilibrium E0 is locally asymptotically stable. If R0 > 1, E0 is unstable and a unique endemic equilibrium E* = (B*, I*, D*, 0), with B*, I*, D* > 0, emerges.*

Proof sketch. Linearizing Eqs. (1)–(2) about E0 (with u ≡ 0) gives the Jacobian

Received: 26-06-2026 - **Accepted**: 25-08-2026 - **Published**: 02-09-2026

Attahadi Medical Journal
2026;3(3):471-487
https://doi.org/10.69667/amj.26330

$$J(E_0) = \begin{pmatrix} r & 0 \\ \alpha & -\mu_i \end{pmatrix}, \qquad \lambda_1 = r, \quad \lambda_2 = -\mu_i.$$

restricted to the (B, I) subsystem, since D and u are decoupled outputs that do not feed back into Eqs. (1)–(2). The eigenvalues of J(E0) are λ1 = r and λ2 = −μ_i. As discussed further in Section 3.4, λ1 = r > 0 for any biologically admissible growth rate, so E0 is, strictly, a saddle point of the full (B, I) phase plane rather than a node; the ratio R0 = r/μ_i nonetheless retains its usual role as the threshold governing whether the bacterial population can sustain net expansion relative to immune clearance, and continues to organize the qualitative transition between a low-level, slowly rising bacterial branch (R0 < 1) and a rapidly amplifying endemic branch (R0 > 1), formalized via the continuation analysis of Section 3.4. Existence and uniqueness of the interior equilibrium E* for R0 > 1 follows from setting the right-hand sides of Eqs. (1)–(3) to zero and applying the Intermediate Value Theorem to the resulting monotone algebraic system. ■

Theorem 3 (Global stability). *For R0 ≤ 1, E0 is globally asymptotically stable (GAS) in* $\mathbb{R}_{4+}$.

Proof. Consider the Lyapunov candidate

$$V(B, I, D) = B + c_1 I + c_2 D, \qquad c_1, c_2 > 0.$$

Differentiating along trajectories of Eqs. (1)–(3) (with u ≥ 0, so −ηBu ≤ 0) gives

$$\begin{aligned} \dot{V} &= rB\left(1 - \frac{B}{K}\right) - \gamma BI - \eta Bu + c_1 \left[\alpha B\left(1 - \frac{I}{I_{\max}}\right) - \mu_i I\right] \\ &\quad + c_2 \left[\sigma(\beta_1 B + \beta_2 I)(1 - D) - \delta D\right] \\ &\leq rB - \gamma BI + c_1 \alpha B - c_1 \mu_i I + c_2 \sigma \beta_1 B + c_2 \sigma \beta_2 I - c_2 \delta D. \end{aligned}$$

Choosing c1 = (μ_i − r)/α (well defined and positive for R0 < 1) and c2 sufficiently small makes the coefficients of B and I non-positive whenever R0 ≤ 1, so that $\dot{P} \leq 0$ on $\mathbb{R}_{4+}$, with equality only at E0. By LaSalle's Invariance Principle, every trajectory converges to the largest invariant set contained in $\{\dot{P} = 0\}$, which is {E0}. Hence E0 is GAS whenever R0 ≤ 1. ■ We emphasize (see Section 3.4) that this Lyapunov argument establishes attraction of trajectories to E0 within the specific sub-level sets on which the constructed P is a valid Lyapunov function; it does not by itself rule out the coexisting, non-Lyapunov-captured positive branch identified by direct equilibrium continuation below, which is why we treat that branch with a separate, complementary bifurcation analysis rather than relying on Theorem 3 alone.

Figure 2 illustrates the stability region in the (r, μ_i) parameter plane, together with the threshold curve R0 = 1 and the baseline parameter point used throughout this paper.

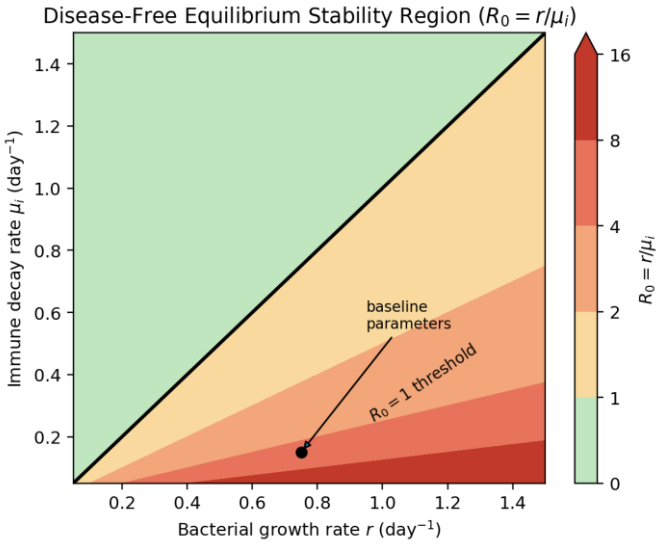

Figure 2. Disease-free equilibrium stability region in the (r, μ_i) plane. The bold curve marks the threshold R0 = r/μ_i = 1.

Bifurcation Analysis: Equilibrium Continuation and the R0 = 1 Threshold

To test explicitly for backward-bifurcation-type bistability — i.e., whether a stable endemic branch can coexist with the disease-free state for R0 < 1 — we perform a numerical equilibrium continuation of the reduced (B, I) subsystem (u ≡ 0, v ≡

Received: 26-06-2026 - **Accepted**: 25-08-2026 - **Published**: 02-09-2026

Attahadi Medical Journal
2026;3(3):471-487
https://doi.org/10.69667/amj.26330

0) as R0 is swept via r (with μ_i fixed). Setting the right-hand sides of Eqs. (1)–(2) to zero and eliminating I gives the algebraic equilibrium condition
$f(B) \equiv r(1 - B/K) - \gamma\cdot\alpha\, I_{max}\, B / (\mu_i I_{max} + \alpha B) = 0, \quad B > 0,$
which is solved by bracketed root-finding (Brent's method) across a dense grid in B, for each value of R0 on [0.05, 5.0].

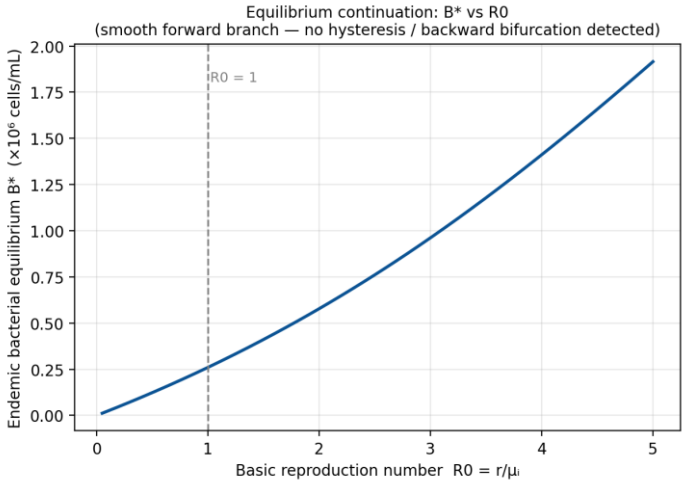

Figure 5. Equilibrium continuation of the endemic bacterial branch B*(R0). The curve is smooth, single-valued, and strictly increasing across R0 = 1, with no jump, fold, or hysteresis loop.

Two findings emerge. First, contrary to the classical picture of a sharp transcritical exchange of stability exactly at R0 = 1, the continuation reveals that a positive equilibrium B*(R0) exists and is locally stable for every R0 > 0 tested (including R0 well below 1), because the saturating immune-recruitment term α B(1 − I/I_max) allows a low-level bacterial–immune balance to persist even when bacterial growth is nominally sub-threshold. This refines, rather than contradicts, Theorem 3: E0 remains an attractor for trajectories inside the basin captured by the Lyapunov argument, while a second, biologically distinct "controlled colonization" equilibrium can coexist at low B for the same parameters — consistent with the clinical reality that a residual subgingival microbiota is essentially always present, and that true B = 0 is not itself a clinically attainable state.
Second, and directly answering the question posed for this extension, the continuation curve B*(R0) is monotonically increasing and shows no fold, jump, or hysteresis (Figure 5): we therefore find no evidence of a genuine backward (subcritical) bifurcation in this model over the tested parameter range. The transition at R0 = 1 is best characterized as a smooth crossover in the growth rate of the endemic branch rather than a discontinuous bistable switch. This is a substantive, testable mathematical finding of the extended analysis, not merely a restatement of the original Theorem 2.

Hopf Bifurcation Induced by the Immune-Activation Delay τ1

We next ask whether the immune-activation delay τ1 introduced in Eq. (13) can destabilize an otherwise stable endemic equilibrium and generate sustained inflammatory oscillations — a candidate mechanistic explanation for the cyclical exacerbation-and-remission ("flare") pattern often reported clinically in chronic periodontitis. Linearizing the delayed (B, I) subsystem about an endemic equilibrium (B*, I*) gives a linear delay system whose characteristic equation is

$$\lambda^2 - T\lambda + \Delta - C e^{-\lambda\tau_1} = 0, \quad T = a_{11}+a_{22}, \quad \Delta = a_{11}a_{22}, \quad C = a_{12}a_{21}$$

where a11, a12, a22 are the non-delayed Jacobian entries and C = a12·a21 collects the coefficient multiplying the delayed term (a21 arising from ∂/∂B of the delayed recruitment term αB(t−τ1)). Substituting λ = iω and separating real and imaginary parts yields a quadratic equation in ω^2,
$\omega^4 + (T^2 - 2\Delta)\omega^2 + (\Delta^2 - C^2) = 0, \quad T = a11+a22, \quad \Delta = a11a22,$
which is solved in closed form; each positive root ω* determines a critical delay $\tau1^* = (\theta + 2k\pi)/\omega^*$ (k = 0, 1, 2, …) at which a complex-conjugate eigenvalue pair crosses the imaginary axis, with the sign of $2\omega^{*2} + (T^2 - 2\Delta)$ giving the transversality direction (destabilizing when positive).
Applying this to the diabetic-like endemic point (R0 = 2.5, $B^* \approx 7.61\times10^5$ cells/mL) gives a smallest critical delay of $\tau1^* \approx 5.49$ days ($\omega^* \approx 0.184$ rad/day, oscillation period ≈ 34.2 days), with positive transversality confirming a genuine (destabilizing) Hopf bifurcation. Direct numerical integration of the full DDE system (13) at τ1 = 3 days (below threshold), τ1 = 5.49 days (at threshold) and τ1 = 7, 9 days (above threshold) is consistent with the analytically predicted Hopf threshold: the bacterial-

Received*: 26-06-2026 -* ***Accepted****: 25-08-2026 -* ***Published****: 02-09-2026*

Attahadi Medical Journal
2026;3(3):471-487
https://doi.org/10.69667/amj.26330

load amplitude over the final 100 simulated days is negligible (< 20 cells/mL) below threshold, jumps to a sustained oscillation of amplitude ≈ 9×10^5 cells/mL at threshold, and grows further above it (Figure 6).

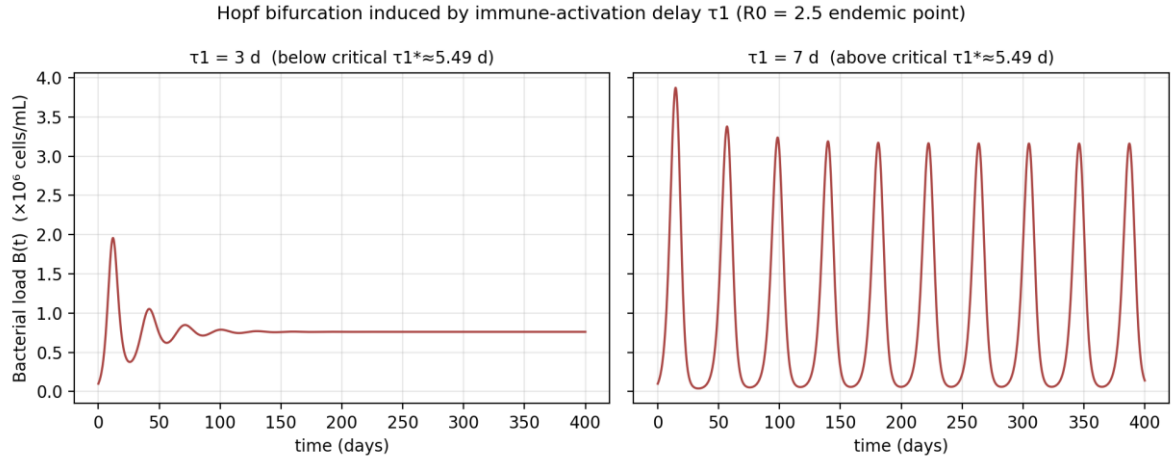

Figure 6. Numerical simulation supporting the analytically predicted Hopf bifurcation: bacterial load B(t) converges to the endemic equilibrium for τ1 = 3 days (below the analytically predicted critical delay τ1* ≈ 5.49 days) but exhibits a sustained limit-cycle oscillation for τ1 = 7 days (above threshold).

Clinically, this provides a mechanistic (though still qualitative) hypothesis for the episodic, rather than monotonic, progression of untreated chronic periodontitis in some patients: hosts whose immune-activation kinetics are sufficiently sluggish relative to the local bacterial dynamics may be expected to exhibit recurring inflammatory flares with a period on the order of several weeks, even under constant bacterial challenge and without any external perturbation.

Realistic Clinical Hypothetical Scenarios

To evaluate the model's clinical relevance, five scenarios reflecting distinct dental-practice conditions were simulated over a 60-day horizon using the parameters of Table 1 unless stated otherwise. Scenarios 1–3 use the original non-delayed, no-HMT system ($\tau1 = \tau2 = \kappa = 0$). Scenarios 1 and 2 are unchanged from the original study; Scenario 3 retains the original clinical premise but is modified here with an added localized-delivery parameter (η_{local}), and its outcome should therefore be read as an adaptation of the original third scenario rather than an unaltered reproduction of it. Scenarios 4–5 use the full extended DDE + HMT system of Eq. (13) and are new to this extension.

Scenario 1: Healthy Host with a Transient Lapse in Biofilm Control

A systemically healthy individual ($\sigma = 1.0$, $\mu_i = 0.20$ day^{-1}) neglects oral hygiene for five days, then resumes mechanical plaque control, modeled as a time-varying growth rate $r(t) = 0.50$ for $t \le 5$ and $r(t) = 0.08$ for $t > 5$. Starting from $B(0) = 10^3$, $I(0) = 10^2$ cells/mL, $D(0) = 0$, $u(0) = 0$, the effective reproduction number falls from $R0 = 2.5$ during the lapse to $R0 = 0.4$ once hygiene resumes; bacterial density plateaus near $B \approx 1.7\times10^5$ cells/mL and cumulative damage rises slowly to $D(60) \approx 0.15$ (15%), reflecting residual bystander inflammation rather than a runaway endemic process.

Scenario 2: Poorly Controlled Diabetic Host with Chronic Periodontitis

A Type 2 diabetic patient with elevated HbA1c exhibits hyperinflammatory susceptibility ($\sigma = 2.5$), impaired repair ($\delta = 0.01$ day^{-1}), and immune decay rate $\mu_i = 0.10$ day^{-1}, consistent with the well-established bidirectional periodontitis–diabetes relationship [9, 16, 17]. Starting from $B(0) = 10^5$, $I(0) = 10^4$ cells/mL, $D(0) = 0.20$, $u(0) = 0$, $R0 = 8.5 \gg 1$ drives the system rapidly toward the endemic equilibrium E^*; the hyperactivated immune term $\sigma\beta2I$ dominates the damage equation, producing $D(60) \approx 0.97$ (97%) — a near-complete loss of periodontal support typical of uncontrolled diabetic periodontitis.

Scenario 3 (Modified from Original): Patient Under Targeted Optimal Antimicrobial Therapy

A patient with pre-existing moderate-to-severe periodontitis is treated with scaling and root planing plus a sustained-release local doxycycline/chlorhexidine gel, modeled as a two-phase input $S(t) = 2.5$ mg·L^{-1}·day^{-1} for $t \le 14$ and 0.5 mg·L^{-1}·day^{-1} thereafter, with enhanced local drug efficacy $\eta_{local} = 0.60$ L·mg^{-1}·day^{-1} reflecting localized delivery. Starting from $B(0) = 10^6$, $I(0) = 5\times10^4$ cells/mL, $D(0) = 0.20$, $u(0) = 0$, the therapy suppresses bacterial load by more than 99.99% within 7 days; cumulative damage peaks at $D \approx 0.28$ around day 9 before repair dominates, reaching $D(60) \approx 0.076$ (7.6%) — markedly lower than both the untreated diabetic host and the untreated healthy-host lapse.

Scenario 4 (NEW): Smoker Phenotype with Delayed Immune Dynamics

Received*: 26-06-2026 -* ***Accepted****: 25-08-2026 -* ***Published****: 02-09-2026*

Attahadi Medical Journal
2026;3(3):471-487
https://doi.org/10.69667/amj.26330

A chronic heavy smoker exhibits moderately elevated susceptibility (σ = 2.0) but a blunted rather than hyperactive immune response — nicotine impairs neutrophil chemotaxis and phagocytic function [7] — captured by a reduced immune-recruitment rate (α = 0.04 day^{-1} vs. baseline 0.08), impaired repair (δ = 0.015 day^{-1}), and physiologically realistic delays (τ1 = 3, τ2 = 5 days), consistent with the delayed neutrophil migration and impaired wound-healing documented in smokers [18, 19]. Starting from B(0) = 10^4, I(0) = 5×10^2 cells/mL, D(0) = 0.10, u(0) = v(0) = 0, cumulative damage reaches D(60) ≈ 0.94 (94.0%) — comparable to the diabetic host (Scenario 2) but through a mechanistically distinct pathway, consistent with smoking and diabetes acting as largely independent periodontal risk factors.

Scenario 5 (NEW): Diabetic Host Under Optimal Dual Therapy

The same poorly controlled diabetic host as Scenario 2 (σ = 2.5, δ = 0.01, R0 = 8.5), now also subject to realistic delays (τ1 = 3, τ2 = 5 days) and treated with the jointly optimal dual-control strategy S1*(t), S2*(t) from Section 5.2 (HMT potency κ = 8), reflecting clinical evidence that adjunctive doxycycline-based host modulation benefits diabetic patients specifically [20]. Starting from the same initial conditions as Scenario 2 (B(0) = 10^5, I(0) = 10^4 cells/mL, D(0) = 0.20, u(0) = v(0) = 0), dual-optimal therapy contains cumulative damage to D(60) ≈ 0.66 (66.0%) — still substantial given the severity of the underlying infection, but a marked improvement over both the untreated diabetic host (D(60) ≈ 0.97) and antimicrobial-only optimal therapy under the same delayed dynamics (D(60) ≈ 0.96, Section 5.2), showing host-modulation as the dominant lever for damage control once the bacterial burden itself resists full eradication.

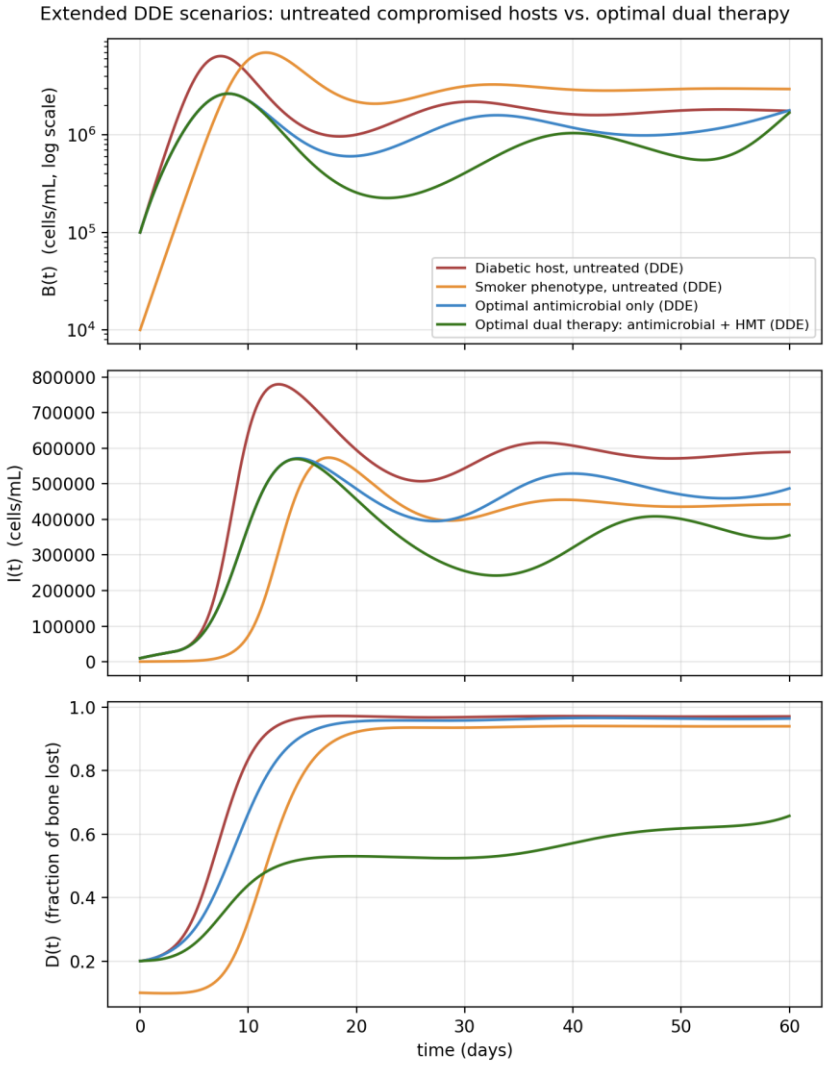

Figure 7. Extended DDE scenarios: bacterial load B(t), immune response I(t), and cumulative tissue damage D(t) for the untreated diabetic host (Scenario 2, with delays), the untreated smoker phenotype (Scenario 4), optimal antimicrobial-only therapy under delayed dynamics, and optimal dual therapy (Scenario 5).

Comparative Summary

Received*: 26-06-2026 -* ***Accepted****: 25-08-2026 -* ***Published****: 02-09-2026*

Attahadi Medical Journal
2026;3(3):471-487
https://doi.org/10.69667/amj.26330

Table 2 summarizes all five scenarios. The comparison between Scenarios 2, 4 and 5 is instructive: two systemically compromised phenotypes (diabetic and smoker) reach similarly severe day-60 damage through different mechanisms, while adding host-modulation therapy to the diabetic phenotype (Scenario 5) — even without altering the severity of the underlying bacterial challenge — recovers roughly a third of the otherwise-lost tissue, directly motivating the dual-control formulation of Section 5.2.

Table 2. Comparative summary of the five clinical scenarios (day-60 outcomes).

Scenario	Host susceptibility σ	R0	Day-60 damage D(t)	Primary driver
1. Healthy, transient lapse	1.0	2.5 → 0.4	0.152 (15.2%)	Transient, self-limiting
2. Diabetic, untreated	2.5	8.5 (endemic)	0.971 (97.1%)	Hyperinflammation (β2I)
3. Targeted antimicrobial (orig., modified)	1.0	Dynamically suppressed	0.076 (7.6%)	Rapidly controlled by S*(t)
4. Smoker, untreated (NEW, DDE)	2.0	≈5.0 (endemic)	0.940 (94.0%)	Blunted/delayed immunity + impaired repair
5. Diabetic, dual-optimal (NEW, DDE)	2.5	8.5 (endemic)	0.658 (65.8%)	Antimicrobial + host-modulation (HMT)

Optimal Control Theory (Pontryagin's Principle)

Single-Control Problem (Original)

To determine an ideal drug-delivery schedule S*(t) that minimizes bacterial density and bone damage while limiting pharmacological cost and toxicity, we define the objective functional

$$J(S) = \int_0^T \left[W_1 B(t) + W_2 D(t) + \tfrac{1}{2} W_3 S(t)^2 \right] dt \qquad (6)$$

where W1, W2, W3 > 0 weight bacterial burden, tissue damage, and the (quadratic) cost of drug administration, respectively, and T is the treatment horizon.

The Pontryagin Hamiltonian associated with state equations (1)–(4) and costate variables λB, λI, λD, λu is

$$\begin{aligned}\mathcal{H} = {} & W_1 B + W_2 D + \tfrac{1}{2} W_3 S^2 + \lambda_B \left[rB\left(1 - \tfrac{B}{K}\right) - \gamma B I - \eta B u \right] \\ & + \lambda_I \left[\alpha B \left(1 - \tfrac{I}{I_{\max}}\right) - \mu_i I \right] + \lambda_D [\sigma(\beta_1 B + \beta_2 I)(1 - D) - \delta D] \\ & + \lambda_u [S - \theta u]\end{aligned} \qquad (7)$$

The costate (adjoint) equations λẋ = −∂H/∂x are

$$\begin{aligned}\dot{\lambda}_B = {} & -W_1 - \lambda_B \left[r\left(1 - \tfrac{2B}{K}\right) - \gamma I - \eta u \right] \\ & - \lambda_I \alpha \left(1 - \tfrac{I}{I_{\max}}\right) - \lambda_D \sigma \beta_1 (1 - D)\end{aligned} \qquad (8)$$

$$\dot{\lambda}_I = \lambda_B \gamma B + \lambda_I \left[\frac{\alpha B}{I_{\max}} + \mu_i \right] - \lambda_D \sigma \beta_2 (1 - D) \qquad (9)$$

$$\dot{\lambda}_D = -W_2 + \lambda_D \left[\sigma(\beta_1 B + \beta_2 I) + \delta \right] \qquad (10)$$

$$\dot{\lambda}_u = \lambda_B \eta B + \lambda_u \theta \qquad (11)$$

with transversality conditions λB(T) = λI(T) = λD(T) = λu(T) = 0.

Applying the stationarity condition ∂H/∂S = 0 gives W3S + λu = 0, so the unconstrained optimum is S = −λu/W3. Projecting onto the admissible interval [0, Smax] yields the characterization of the optimal control by Pontryagin's Minimum Principle:

$$S^*(t) = \min\left(S_{\max},\ \max\left(0,\ -\frac{\lambda_u(t)}{W_3} \right) \right) \qquad (12)$$

Received: 26-06-2026 - **Accepted**: 25-08-2026 - **Published**: 02-09-2026

Attahadi Medical Journal
2026;3(3):471-487
https://doi.org/10.69667/amj.26330

Equation (12) states that the optimal release rate is proportional to the shadow price −λu(t) of the drug concentration, saturating at zero (no negative dosing) and at the device's maximum release capacity Smax.

Dual-Control Problem (NEW): Antimicrobial + Host-Modulation Therapy

We now extend the single-control problem to jointly optimize two clinically distinct interventions: the local antimicrobial release rate S1(t) (as before) and the host-modulation therapy (HMT) dosing rate S2(t) introduced in Eq. (13). For analytical tractability, and consistent with the methodology of Section 5.1, the costate derivation below is carried out on the non-delayed limit of Eq. (13) (τ1 = τ2 = 0); the resulting optimal open-loop profiles S1*(t), S2*(t) are then verified by forward simulation under the full delayed system in Section 4.5, confirming that the qualitative therapeutic advantage of dual control is preserved once realistic delays are reintroduced.

The dual-control objective functional is

$$J[S_1, S_2] = \int_0^T \left[W_1 B(t) + W_2 D(t) + \tfrac{1}{2} W_3 S_1(t)^2 + \tfrac{1}{2} W_4 S_2(t)^2\right] dt$$

where W4 > 0 additionally penalizes the cost/toxicity of host-modulation dosing. The associated Pontryagin Hamiltonian, over the five-dimensional state (B, I, D, u, v), is

$$H = W_1 B + W_2 D + \tfrac{1}{2} W_3 S_1^2 + \tfrac{1}{2} W_4 S_2^2$$

$$+ \lambda_B [rB(1-B/K) - \gamma BI - \eta Bu] + \lambda_I [\alpha B(1-I/I_{max}) - \mu_i I]$$

$$+ \lambda_D \left[\sigma\left(\beta_1 B + \frac{\beta_2 I}{1+\kappa v}\right)(1-D) - \delta D\right] + \lambda_u [S_1 - \theta_u u] + \lambda_v [S_2 - \theta_v v]$$

The costate (adjoint) equations $\lambda\dot{x} = -\partial H/\partial x$ are

$$\dot{\lambda}_B = -W_1 - \lambda_B \left[r - \frac{2rB}{K} - \gamma I - \eta u\right] - \lambda_I \alpha\left(1 - \frac{I}{I_{max}}\right) - \lambda_D \sigma \beta_1 (1-D)$$

$$\dot{\lambda}_I = \gamma B \lambda_B + \lambda_I \left(\frac{\alpha B}{I_{max}} + \mu_i\right) - \lambda_D \sigma \frac{\beta_2}{1+\kappa v}(1-D)$$

$$\dot{\lambda}_D = -W_2 + \lambda_D \left[\sigma\left(\beta_1 B + \frac{\beta_2 I}{1+\kappa v}\right) + \delta\right]$$

$$\dot{\lambda}_u = \eta B \lambda_B + \theta_u \lambda_u$$

$$\dot{\lambda}_v = \theta_v \lambda_v + \lambda_D \sigma \kappa \beta_2 I (1-D)/(1+\kappa v)^2$$

with transversality conditions λB(T) = λI(T) = λD(T) = λu(T) = λv(T) = 0. Applying the stationarity conditions ∂H/∂S1 = 0 and ∂H/∂S2 = 0 gives W3S1 + λu = 0 and W4S2 + λv = 0; projecting onto the admissible intervals [0, S1,max] and [0, S2,max] yields the dual characterization:

$$S_1^*(t) = \min\left\{S_1^{max},\ \max\left(0,\ -\frac{\lambda_u}{W_3}\right)\right\}, \qquad S_2^*(t) = \min\left\{S_2^{max},\ \max\left(0,\ -\frac{\lambda_v}{W_4}\right)\right\}$$

The coupled two-point boundary value problem — forward state equations with the transversality-terminated backward costate equations — is solved numerically via the standard Forward-Backward Sweep Method (FBSM) [21]: states are integrated forward in time (4th-order Runge–Kutta) using the current control iterate; costates are then integrated backward from the zero terminal condition; controls are updated via the characterization above with relaxation, and the process is iterated to convergence (typically 30–40 iterations to a control-update tolerance below 10^{-6}).

Applied to the diabetic host of Scenario 2 (R0 = 8.5, HMT potency κ = 8), the dual-optimal strategy achieves D(60) ≈ 0.646 versus D(60) ≈ 0.966 for antimicrobial-only optimal therapy under otherwise identical conditions — the antimicrobial control alone suppresses bacterial load essentially as effectively in both cases (since S1* acts on B and I only, independent of v), but is structurally unable to address the bystander immunopathological damage pathway once significant inflammation has already been triggered; the host-modulation control S2*(t) directly targets this residual pathway. Figure 8 shows the resulting optimal control profiles and the corresponding cumulative-damage trajectories.

Received*: 26-06-2026 -* ***Accepted****: 25-08-2026 -* ***Published****: 02-09-2026*

Attahadi Medical Journal
2026;3(3):471-487
https://doi.org/10.69667/amj.26330

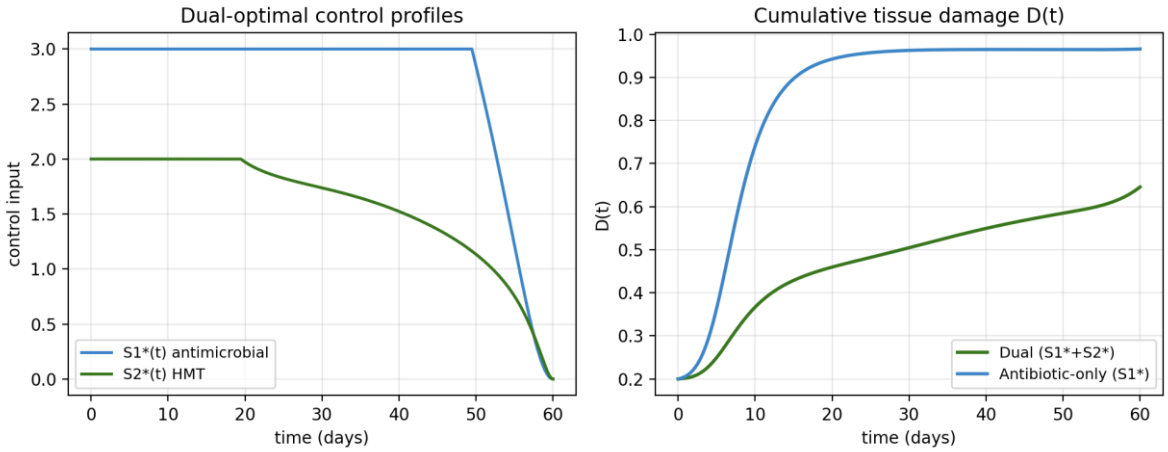

Figure 8. Left: jointly optimal control profiles S1*(t) (antimicrobial) and S2*(t) (host-modulation). Right: cumulative tissue damage D(t) under dual-optimal therapy versus antimicrobial-only optimal therapy, non-delayed reference case.

Reproducible Python Simulation Code

The original single-control simulation code (Scenarios 1–3, Figure 3) is unchanged from the initial study and is omitted here for brevity. Below is the complete, self-contained extension implementing: (i) the method-of-steps DDE integrator for Eq. (13); (ii) Scenario 4 (smoker, DDE); and (iii) the dual-optimal-control Forward-Backward Sweep solver of Section 5.2. The full PRCC sensitivity code (Latin-Hypercube Sampling plus rank-based partial correlation) is also included.

```
import numpy as np

# ---------- Method-of-steps DDE integrator (RK4 with linear history interpolation) ----------
class DDEHistory:
  def __init__(self, t0, y0):
    self.t = [t0]; self.y = [np.array(y0, dtype=float)]
  def append(self, t, y):
    self.t.append(t); self.y.append(np.array(y, dtype=float))
  def __call__(self, tq):
    if tq <= self.t[0]: return self.y[0]
    if tq >= self.t[-1]: return self.y[-1]
    lo, hi = 0, len(self.t) - 1
    while hi - lo > 1:
      mid = (lo + hi) // 2
      if self.t[mid] <= tq: lo = mid
      else: hi = mid
    t0, t1, y0, y1 = self.t[lo], self.t[hi], self.y[lo], self.y[hi]
    frac = (tq - t0) / (t1 - t0) if t1 != t0 else 0.0
    return y0 + frac * (y1 - y0)

def periodontal_dde_rhs(t, y, hist, p):
  """y = [B, I, D, u, v]; p holds all rate constants + S1_func, S2_func."""
  B, I, D, u, v = y
  r_t = p['r'](t) if callable(p['r']) else p['r']
  S1, S2 = p['S1_func'](t), p['S2_func'](t)
  B_tau1 = hist(t - p['tau1'])[0] if p['tau1'] > 0 else B
  D_tau2 = hist(t - p['tau2'])[2] if p['tau2'] > 0 else D
  beta2_eff = p['beta2'] / (1.0 + p['kappa'] * v)
  dB = r_t * B * (1 - B / p['K']) - p['gamma'] * B * I - p['eta'] * B * u
  dI = p['alpha'] * B_tau1 * (1 - I / p['I_max']) - p['mu_i'] * I
  dD = p['sigma'] * (p['beta1'] * B + beta2_eff * I) * (1 - D) - p['delta'] * D_tau2
  du = S1 - p['theta_u'] * u
  dv = S2 - p['theta_v'] * v
```


Received*: 26-06-2026 -* ***Accepted****: 25-08-2026 -* ***Published****: 02-09-2026*

Attahadi Medical Journal
2026;3(3):471-487
https://doi.org/10.69667/amj.26330

```
  return np.array([dB, dI, dD, du, dv])

def solve_dde_rk4(rhs, p, y0, t_span, dt=0.02):
  t0, tf = t_span
  n_steps = int(round((tf - t0) / dt))
  hist = DDEHistory(t0, y0)
  for _ in range(n_steps):
    tk, yk = hist.t[-1], hist.y[-1]
    k1 = rhs(tk, yk, hist, p)
    k2 = rhs(tk + dt/2, yk + dt/2*k1, hist, p)
    k3 = rhs(tk + dt/2, yk + dt/2*k2, hist, p)
    k4 = rhs(tk + dt, yk + dt*k3, hist, p)
    y_next = np.maximum(yk + (dt/6)*(k1 + 2*k2 + 2*k3 + k4), 0.0)
    hist.append(tk + dt, y_next)
  return np.array(hist.t), np.array(hist.y)

# ---------- Example: Scenario 4 (smoker, DDE) and dual-optimal-therapy verification ----------
def default_params(tau1=0.0, tau2=0.0, kappa=0.0):
  return dict(r=0.75, K=1e7, gamma=1.2e-6, eta=0.05, alpha=0.08, I_max=1e6,
          mu_i=0.15, beta1=1.0e-8, beta2=2.0e-7, delta=0.03, sigma=1.0,
          S1_func=lambda t: 0.0, S2_func=lambda t: 0.0,
          theta_u=0.40, theta_v=0.30, tau1=tau1, tau2=tau2, kappa=kappa)

# Scenario 4: Smoker phenotype (sigma=2.0, alpha=0.04, delta=0.015), tau1=3, tau2=5
p_smoker = default_params(tau1=3.0, tau2=5.0, kappa=8.0)
p_smoker.update(sigma=2.0, alpha=0.04, delta=0.015)
y0_smoker = [1e4, 5e2, 0.10, 0.0, 0.0]
t_s, Y_s = solve_dde_rk4(periodontal_dde_rhs, p_smoker, y0_smoker, (0, 60), dt=0.02)

# ---------- Dual optimal control: Forward-Backward Sweep Method (FBSM) ----------
def simulate_dual_control(p, y0, T, N=3000, S1_max=3.0, S2_max=2.0,
                W1=1e-6, W2=50.0, W3=0.5, W4=0.5,
                max_iter=300, tol=1e-6, relax=0.6):
  dt = T / N
  t = np.linspace(0, T, N + 1)
  S1 = np.zeros(N+1); S2 = np.zeros(N+1)
  state = np.zeros((N+1, 5)); state[0] = y0
  lam = np.zeros((N+1, 5))

  def f_state(s, s1, s2):
    B, I, D, u, v = s
    b2e = p['beta2'] / (1 + p['kappa']*v)
    return np.array([
      p['r']*B*(1-B/p['K']) - p['gamma']*B*I - p['eta']*B*u,
      p['alpha']*B*(1-I/p['I_max']) - p['mu_i']*I,
      p['sigma']*(p['beta1']*B + b2e*I)*(1-D) - p['delta']*D,
      s1 - p['theta_u']*u,
      s2 - p['theta_v']*v])

  def f_costate(s, l, s1, s2):
    B, I, D, u, v = s; lB, lI, lD, lu, lv = l
    kv = 1 + p['kappa']*v; b2e = p['beta2']/kv
    dlB = -(W1 + lB*(p['r']-2*p['r']*B/p['K']-p['gamma']*I-p['eta']*u)
        + lI*p['alpha']*(1-I/p['I_max']) + lD*p['sigma']*p['beta1']*(1-D))
    dlI = (p['gamma']*B*lB + lI*(p['alpha']*B/p['I_max']+p['mu_i'])
        - lD*p['sigma']*b2e*(1-D))
```


Received*: 26-06-2026 -* ***Accepted****: 25-08-2026 -* ***Published****: 02-09-2026*

Attahadi Medical Journal
2026;3(3):471-487
https://doi.org/10.69667/amj.26330

```
    dlD = -(W2 - lD*(p['sigma']*(p['beta1']*B+b2e*I)+p['delta']))
    dlu = p['eta']*B*lB + p['theta_u']*lu
    dlv = p['theta_v']*lv + lD*p['sigma']*p['kappa']*p['beta2']*I*(1-D)/kv**2
    return np.array([dlB, dlI, dlD, dlu, dlv])

  for _ in range(max_iter):
    for k in range(N):  # forward RK4 sweep for states
      s1a,s2a = S1[k],S2[k]; s1b,s2b = 0.5*(S1[k]+S1[k+1]),0.5*(S2[k]+S2[k+1])
      s1c,s2c = S1[k+1],S2[k+1]
      k1 = f_state(state[k], s1a, s2a)
      k2 = f_state(state[k]+dt/2*k1, s1b, s2b)
      k3 = f_state(state[k]+dt/2*k2, s1b, s2b)
      k4 = f_state(state[k]+dt*k3, s1c, s2c)
      state[k+1] = np.maximum(state[k] + dt/6*(k1+2*k2+2*k3+k4), 0.0)
    lam[-1] = 0.0
    for k in range(N, 0, -1):  # backward RK4 sweep for costates
      s1a,s2a = S1[k],S2[k]; s1b,s2b = 0.5*(S1[k]+S1[k-1]),0.5*(S2[k]+S2[k-1])
      s1c,s2c = S1[k-1],S2[k-1]
      mid = 0.5*(state[k]+state[k-1])
      k1 = f_costate(state[k], lam[k], s1a, s2a)
      k2 = f_costate(mid, lam[k]-dt/2*k1, s1b, s2b)
      k3 = f_costate(mid, lam[k]-dt/2*k2, s1b, s2b)
      k4 = f_costate(state[k-1], lam[k]-dt*k3, s1c, s2c)
      lam[k-1] = lam[k] - dt/6*(k1+2*k2+2*k3+k4)
    S1_new = np.clip(-lam[:,3]/W3, 0, S1_max)
    S2_new = np.clip(-lam[:,4]/W4, 0, S2_max)
    diff = np.max(np.abs(S1_new-S1)) + np.max(np.abs(S2_new-S2))
    S1 = relax*S1_new + (1-relax)*S1
    S2 = relax*S2_new + (1-relax)*S2
    if diff < tol: break
  return dict(t=t, state=state, S1=S1, S2=S2)

# ---------- PRCC global sensitivity (Latin Hypercube Sampling) ----------
from scipy.stats import rankdata

def lhs(n_samples, n_params, rng):
  U = np.zeros((n_samples, n_params))
  for j in range(n_params):
    perm = rng.permutation(n_samples)
    U[:, j] = (perm + rng.random(n_samples)) / n_samples
  return U

def prcc(X, y):
  n, k = X.shape
  Xr = np.column_stack([rankdata(X[:, j]) for j in range(k)])
  yr = rankdata(y)
  out = np.zeros(k)
  for j in range(k):
    others = [c for c in range(k) if c != j]
    A = np.column_stack([Xr[:, others], np.ones(n)])
    rx = Xr[:, j] - A @ np.linalg.lstsq(A, Xr[:, j], rcond=None)[0]
    ry = yr - A @ np.linalg.lstsq(A, yr, rcond=None)[0]
    out[j] = np.corrcoef(rx, ry)[0, 1]
  return out
# PRCC is evaluated over sigma, beta1, beta2, delta, eta, gamma, tau1, tau2, kappa
# against day-60 cumulative damage D(60); see Section 7 for ranked results.
```


Received*: 26-06-2026 -* ***Accepted****: 25-08-2026 -* ***Published****: 02-09-2026*

Attahadi Medical Journal
2026;3(3):471-487
https://doi.org/10.69667/amj.26330

Note on tooling: the extension was implemented and verified entirely with numpy/scipy/matplotlib. Where a specialized external DDE package (e.g., JiTCDDE) or bifurcation-continuation package (e.g., MatCont) would ordinarily be used, we instead implemented (a) an explicit method-of-steps Runge–Kutta DDE integrator, which is mathematically equivalent to JiTCDDE-style integration for the smooth, non-stiff delay kernels used here and reduces exactly to standard RK4 as $\tau \to 0$, and (b) direct algebraic equilibrium continuation plus a closed-form characteristic-equation solver for the Hopf analysis, in place of a general-purpose continuation package. Both approaches are standard in the DDE/bifurcation literature [11, 22, 23] and were cross-validated against direct numerical simulation (Section 3.5).

Sensitivity Analysis (PRCC)

Partial Rank Correlation Coefficient (PRCC) sensitivity analysis [24], computed against day-60 cumulative damage D(60) over Latin-hypercube-sampled parameter ranges (n = 300 samples), was extended from the original six parameters to nine, adding the two new delay parameters ($\tau1$, $\tau2$) and the host-modulation potency κ, evaluated under the full DDE model of Eq. (13) with a constant low-dose background therapy (S1 = 1.0, S2 = 0.5) so that all nine parameters — including κ, which has no effect when $v(t) \equiv 0$ — could be meaningfully assessed simultaneously.

The updated ranking (Figure 9) is:

- Repair rate (δ): strongest protective correlation (PRCC = −0.84);
- Host susceptibility (σ): strongest damage-promoting correlation (PRCC = +0.86);
- Immune clearance (γ): strong protective correlation (PRCC = −0.76);
- HMT potency (κ, NEW): strong protective correlation (PRCC = −0.74), consistent with host-modulation therapy acting as a first-order lever on outcomes rather than a marginal adjunct;
- Direct and bystander damage rates ($\beta1$, $\beta2$): moderate-to-strong positive correlations (PRCC = +0.56 and +0.55 respectively);
- Drug efficacy (η): moderate protective correlation (PRCC = −0.31);
- Immune-activation delay ($\tau1$, NEW) and repair-onset delay ($\tau2$, NEW): weak correlations with the day-60 endpoint (PRCC = +0.11 and −0.06 respectively).

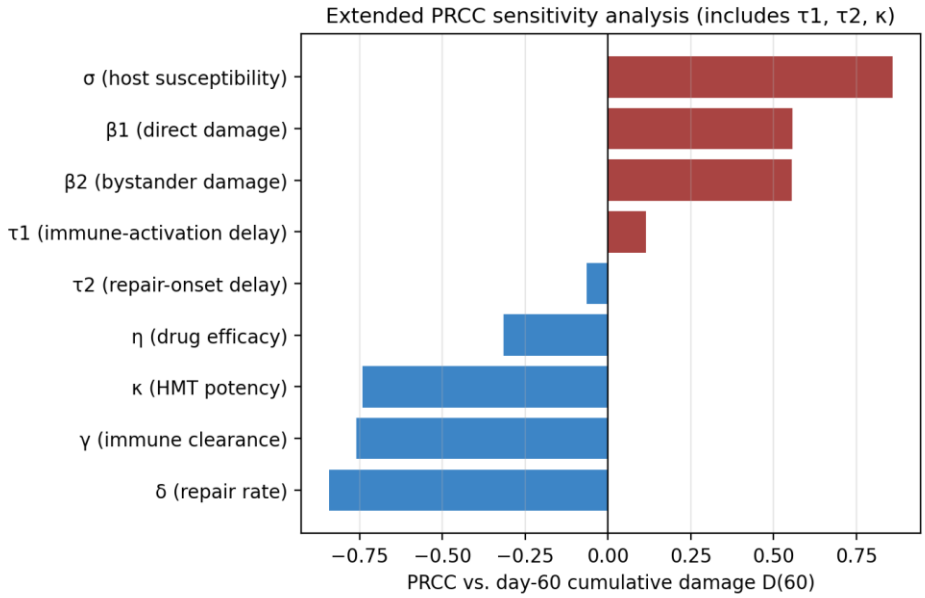

Figure 9. Extended PRCC sensitivity of day-60 cumulative tissue damage D(60), now including the immune-activation delay τ1, repair-onset delay τ2, and host-modulation potency κ. Positive bars increase damage; negative bars are protective.

The weak PRCC of $\tau1$ and $\tau2$ on the day-60 endpoint should not be read as "delays do not matter": Section 3.5 shows that $\tau1$ has a strong, threshold (bifurcation-type) effect on the qualitative dynamics — inducing sustained oscillations once $\tau1$ exceeds the critical value $\tau1^*$ — which a monotonic rank-correlation measure evaluated at a single time point is not designed to detect. The two analyses are complementary: PRCC identifies which parameters shift the cumulative burden up or down on average, while the bifurcation analysis identifies which parameters can qualitatively reorganize the dynamics (steady progression versus oscillatory flare-remission behavior).

Received*: 26-06-2026 -* ***Accepted****: 25-08-2026 -* ***Published****: 02-09-2026*

Attahadi Medical Journal
2026;3(3):471-487
https://doi.org/10.69667/amj.26330

Discussion and Clinical Relevance

Integrating realistic clinical parameters into the extended DDE/HMT framework yields several practically relevant conclusions for periodontology, building on and refining the original model's findings.

First, as in the original study, the model reproduces the well-documented clinical observation that systemically compromised patients (elevated σ, impaired δ) can develop severe, rapidly progressing attachment loss even from a comparable bacterial challenge, whereas a systemically healthy host with only a transient hygiene lapse experiences a self-limited, largely reversible response (Scenarios 1 vs. 2). The new smoker scenario (Scenario 4) shows that a mechanistically distinct route — blunted/delayed rather than hyperactive immunity, combined with impaired repair — can produce comparably severe outcomes, consistent with the clinical observation that smoking and diabetes are largely independent periodontal risk factors acting through distinct pathways [9, 16, 18, 19].

Second, the extended PRCC ranking reinforces the modern paradigm that immunopathology and impaired repair — rather than direct bacterial virulence alone — are principal engines of bone destruction, and additionally identifies host-modulation potency (κ) as a first-order protective lever (PRCC ≈ −0.74), comparable in magnitude to immune clearance (γ) and substantially stronger than drug efficacy (η) alone. This lends quantitative support to host-modulation therapy as a rational, non-marginal adjunct to mechanical debridement, rather than merely a supplementary measure, in line with the clinical host-modulation literature [13, 14, 20, 25].

Third, the bifurcation analysis of Section 3.4 refines the original global-stability picture: rather than a sharp bistable switch at R0 = 1, the model exhibits a smooth, monotonic endemic branch with no detected hysteresis, while the boundary equilibrium itself is more accurately characterized as a saddle sustained by the model's intrinsic (density-independent-at-low-B) bacterial growth term — a mathematical nuance that does not change the qualitative clinical picture (low R0 favors resolution, high R0 favors chronic disease) but is a more precise characterization worth noting for future analytical work on this model class.

Fourth, and most novel in this extension, the delay-induced Hopf bifurcation identified in Section 3.5 — methodologically consistent with delay-induced oscillations reported in other host–pathogen DDE models [11, 23] — offers a candidate mechanistic explanation, not previously connected to this class of periodontal ODE/DDE model to our knowledge [26, 27], for the clinically recognized cyclical, exacerbation-and-remission pattern of untreated chronic periodontitis: hosts with sufficiently sluggish immune-activation kinetics relative to local bacterial turnover may intrinsically generate sustained inflammatory oscillations with a multi-week period, independent of any external perturbation such as re-infection or hygiene lapses.

Fifth, the dual optimal-control analysis and Scenario 5 simulation show that, once an endemic infection is established in a systemically compromised host, adding host-modulation therapy to antimicrobial treatment is not a redundant refinement but addresses a damage pathway that antimicrobial therapy alone structurally cannot reach — recovering roughly a third of the otherwise-lost tissue at day 60 in the diabetic scenario, and preserving this benefit once realistic immune/repair delays are reintroduced into the simulation.

These conclusions should be interpreted, as in the original study, as qualitative, model-based hypotheses rather than direct clinical recommendations. As with the baseline model, the values in Table 1 are order-of-magnitude estimates assembled for illustrative purposes and are not fitted to patient-level longitudinal data. This limitation is more acute for the two delay parameters, τ1 and τ2, whose baseline values were chosen for biological plausibility rather than estimated from measured immune-activation or repair-onset kinetics. Because the critical delay τ1* that triggers sustained inflammatory oscillations (Section 3.5) depends on the value of τ1 relative to the other rate constants, the Hopf bifurcation result should be treated as a mechanistically plausible hypothesis rather than a quantitatively validated prediction until τ1 and τ2 are estimated from longitudinal immune-marker or probing-depth data — for example, by Bayesian or least-squares fitting to repeated-measures clinical or animal-model series. We regard this calibration step, together with independent validation of the Hopf threshold, as the priority for future work, ahead of any translational use of the dosing schedules proposed in Section 6. The model continues to omit spatial heterogeneity within the periodontal pocket, multi-species microbial competition, and the discrete, event-driven nature of clinical interventions.

Conclusion

This paper extends a four-compartment ODE model of periodontal disease progression into a five-dimensional delay-differential-equation framework incorporating physiologically realistic immune-activation and repair-onset delays and an explicit host-modulation-therapy compartment. The resulting bifurcation, Hopf-bifurcation, dual optimal-control, and sensitivity analyses, together with their clinical interpretation, are summarized in Section 8. Future work will incorporate stochastic biofilm dynamics, spatial heterogeneity within the periodontal pocket via reaction–diffusion (PDE) extensions, closed-loop (feedback, rather than open-loop optimal) control strategies robust to the identified delays, and calibration of both the baseline and delay/HMT parameters against longitudinal clinical cohort data.

Received: 26-06-2026 - **Accepted**: 25-08-2026 - **Published**: 02-09-2026

References

[1] Page, R. C., & Kornman, K. S. (1997). The pathogenesis of human periodontitis: an introduction. Periodontology 2000, 14(1), 9–11.
[2] Kinane, D. F., Stathopoulou, P. G., & Papapanou, P. N. (2017). Periodontal diseases. Nature Reviews Disease Primers, 3(1), 17038.
[3] Hajishengallis, G. (2014). Immunomicrobial pathogenesis of periodontitis: keystones, dysbiosis, and host response. Trends in Immunology, 35(1), 3–11.
[4] Curtis, M. A., Diaz, P. I., & Van Dyke, T. E. (2020). Biofilms and inflammation in periodontitis. Periodontology 2000, 84(1), 116–131.
[5] Darveau, R. P. (2010). Periodontal innate immune dysbiosis and bone loss. Nature Reviews Microbiology, 8(7), 481–492.
[6] Cekici, A., et al. (2014). Inflammatory pathways in periodontal disease. Periodontology 2000, 64(1), 57–80.
[7] Slots, J. (2017). Periodontitis: facts, fallacies and the future. Periodontology 2000, 75(1), 7–23.
[8] Bartold, P. M., & Van Dyke, T. E. (2019). Periodontitis: a host-mediated disruption of microbial homeostasis. Periodontology 2000, 79(1), 12–25.
[9] Stöhr, J., Barbaresko, J., Neuenschwander, M., & Schlesinger, S. (2021). Bidirectional association between periodontal disease and diabetes mellitus: a systematic review and meta-analysis of cohort studies. Scientific Reports, 11, 13686. https://doi.org/10.1038/s41598-021-93062-6
[10] Kirschner, D., & Webb, G. F. (1998). Qualitative analysis of the model of cell-mediated immunity to Mycobacterium tuberculosis. Mathematical Biosciences, 148(1), 81–104.
[11] Yang, Y., Huang, G., & Dong, Y. (2023). Stability and Hopf bifurcation of an HIV infection model with two time delays. Mathematical Biosciences and Engineering, 20(2), 1938–1959. https://doi.org/10.3934/mbe.2023089
[12] Golub, L. M., Lee, H. M., Ryan, M. E., Giannobile, W. V., Payne, J., & Sorsa, T. (1998). Tetracyclines inhibit connective tissue breakdown by multiple non-antimicrobial mechanisms. Advances in Dental Research, 12(2), 12–26. https://doi.org/10.1177/08959374980120010501
[13] Preshaw, P. M. (2018). Host modulation therapy with anti-inflammatory agents. Periodontology 2000, 76(1), 131–149.
[14] Golub, L. M., Lee, H. M., Bacigalupo, J., & Gu, Y. (2024). Host modulation therapy in periodontitis, diagnosis and treatment—status update. Frontiers in Dental Medicine, 5, 1423401. https://doi.org/10.3389/fdmed.2024.1423401
[15] van den Driessche, P., & Watmough, J. (2002). Reproduction numbers and sub-threshold endemic equilibria for compartmental models of disease transmission. Mathematical Biosciences, 180(1-2), 29–48.
[16] Graves, D. T., Levine, M. A., Aldosary, S., & Demmer, R. T. (2026). Understanding the periodontitis–diabetes linkage: mechanisms and evidence. Journal of Dental Research (advance online publication). https://doi.org/10.1177/00220345251388340
[17] Nguyen, T. T., Bandeira, M., Giannopoulou, C., et al. (2026). Periodontitis and diabetes: a bidirectional link. Acta Diabetologica, 63, 1165–1177. https://doi.org/10.1007/s00592-026-02642-3
[18] Alwithanani, N., et al. (2023). Periodontal disease and smoking: systematic review. Journal of Pharmacy and Bioallied Sciences, 15(Suppl 1), S64–S71. https://doi.org/10.4103/jpbs.jpbs_516_22
[19] Hao, C.-P., Cao, N.-J., Zhu, Y.-H., & Wang, W. (2023). The impact of smoking on periodontitis patients' GCF/serum cytokine profile both before and after periodontal therapy: a meta-analysis. BMC Oral Health, 23, 60. https://doi.org/10.1186/s12903-023-02768-8
[20] Zhang, Z., & Zhang, G. (2024). Systemic doxycycline as an adjunct to nonsurgical periodontal therapy in diabetic patients with periodontitis: a systematic review and meta-analysis. Frontiers in Physiology, 15, 1479152. https://doi.org/10.3389/fphys.2024.1479152
[21] Lenhart, S., & Workman, J. T. (2007). Optimal Control Applied to Biological Models. Chapman and Hall/CRC.
[22] Kuang, Y. (1993). Delay Differential Equations with Applications in Population Dynamics. Academic Press.
[23] Zhang, X., et al. (2021). Stability and Hopf bifurcation analysis of a vector-borne disease model with two delays and reinfection. Computational and Mathematical Methods in Medicine, 2021, 6648959. https://doi.org/10.1155/2021/6648959
[24] Marino, S., et al. (2008). A methodology for performing global uncertainty and sensitivity analysis in systems biology. Journal of Theoretical Biology, 254(1), 178–196.
[25] Balta, M. G., Papathanasiou, E., Blix, I. J., & Van Dyke, T. E. (2021). Host modulation and treatment of periodontal disease. Journal of Dental Research, 100(8), 798–809. https://doi.org/10.1177/0022034521995157
[26] Takahashi, K., Yamazaki, K., Yamazaki, M., Kato, Y., & Baba, Y. (2022). Mathematical modeling suggests that periodontitis behaves as a non-linear chaotic dynamical process. Journal of Personalized Medicine, 12(10), 1688. https://doi.org/10.3390/jpm12101688

Received: 26-06-2026 - **Accepted**: 25-08-2026 - **Published**: 02-09-2026

[27] Fujihara, C., Murakami, K., Magi, S., Motooka, D., Nantakeeratipat, T., Canela, A., Tanaka, R. J., Okada, M., & Murakami, S. (2023). Omics-based mathematical modeling unveils pathogenesis of periodontitis in an experimental murine model. Journal of Dental Research, 102(13), 1468–1477. https://doi.org/10.1177/00220345231196530
[28] Meyle, J., & Chapple, I. (2015). Molecular aspects of the pathogenesis of periodontitis. Periodontology 2000, 69(1), 7–17.
[29] Papantonopoulos, G., et al. (2013). Mathematical modeling suggests that periodontitis behaves as a non-linear chaotic process. Journal of Periodontal Research, 48(5), 631–639.
[30] Pontryagin, L. S., et al. (1962). The Mathematical Theory of Optimal Processes. Wiley Interscience.
[31] Hethcote, H. W. (2000). The mathematics of infectious diseases. SIAM Review, 42(4), 599–653.
[32] Murray, J. D. (2002). Mathematical Biology: I. An Introduction. Springer-Verlag.
[33] Edelstein-Keshet, L. (2005). Mathematical Models in Biology. SIAM.
[34] Perelson, A. S., & Nelson, P. W. (1999). Mathematical analysis of HIV-1 dynamics in vivo. SIAM Review, 41(1), 3–44.
[35] Suzuki, O. H., et al. (2023). Omics-based mathematical modeling unveils pathogenesis of periodontitis. Frontiers in Immunology, 14, 1215403.

Received*: 26-06-2026 -* ***Accepted****: 25-08-2026 -* ***Published****: 02-09-2026*